Secrecy Analysis for Multi-Relaying RF-FSO Systems With a Multi-Aperture Destination

Jiliang Zhang,[1] **Xiaojun Pan**,[1] **Gaofeng Pan**,[2,3] ***Member, IEEE***, **and Yiyuan Xie**,[1] ***Member, IEEE***

[1]Key Laboratory of Networks and Cloud Computing Security of Universities in Chongqing, School of Electronic and Information Engineering, Southwest University, Chongqing 400715, China
[2]School of Information and Electronics Engineering, Beijing Institute of Technology, Beijing 100081, China
[3]Computer, Electrical and Mathematical Sciences and Engineering Division, King Abdullah University of Science and Technology, Thuwal 23955-6900, Saudi Arabia

DOI:10.1109/JPHOT.2020.2983078

Manuscript received December 23, 2019; revised March 14, 2020; accepted March 21, 2020. Date of publication March 30, 2020; date of current version April 16, 2020. Corresponding author: Jiliang Zhang. (email: swuzhang@swu.edu.cn).

Abstract: In this paper, we investigate the physical layer security for an asymmetric dual-hop radio frequency-free space optical (RF-FSO) communication system, in which a source transmits information to a multi-aperture destination (D) through a best relay under the wiretapping of a multi-aperture eavesdropper (E). The best relay is selected by a partial relay selection scheme in terms of maximum instantaneous channel gain for the RF link. Moreover, equal gain combining scheme is also used to process the multiple copies of receiving signal at D and E. Assuming all the RF channels are subject to independent and identical distributed (i.i.d.) Nakagami-*m* fading and all the FSO channels are modeled by i.i.d. Gamma-Gamma process, the secrecy performance in terms of secrecy outage probability and the probability of strictly positive secrecy capacity are studied, and the accuracy of the analytical results is verified by Monte-Carlo simulations.

Index Terms: Multi-aperture, partial relay selection, physical layer security, radio frequency-free space optical (RF-FSO), secrecy outage probability.

1. Introduction

With the growing demand of huge capacity and high data transfer rate of communication networks, free space optical (FSO), which shows several superior characteristics like high data rate, large system capacity, unlicensed spectrum and immunity to electromagnetic interference, has drawn increasingly attention in the past few years [1]. However, the performance of the FSO systems may decrease severely due to the inherent impairments like atmospheric turbulence and pointing errors [2].

To overcome the aforementioned shortage and to extend the application of FSO systems, an asymmetry hybrid RF-FSO system has been proposed in the open literature, as it can take the full advantages of both RF and FSO techniques simultaneously, such as long transmission distance and large capacity [3]–[6]. The authors in [3] proposed a parallel hybrid FSO-RF communication system, in which the information signal was transmitted to a destination simultaneously through

both FSO and RF links, and a selection combining scheme was employed at the receiver to process those signals. In addition, the unified performance, i.e., bit error rate (BER), outage probability (OP), and ergodic capacity (EC), was evaluated. Such performance was also analyzed when taking into account the effects of pointing errors strength, detection techniques, and both fixed and variable gain relay schemes in [4]. In [5], the authors studied the EC for a multi-hop FSO system with an additional RF link, where the RF link was selected to transmit information when the instantaneous signal-to-noise ratio (SNR) of the FSO link is below a pre-defined threshold. Based on the feedback of channel state information (CSI), a switching system between a primary FSO link and a secondary two-hop RF-FSO link were investigated in [6].

On the other hand, the multi-relaying scheme, which has been considered as an effective way to enhance the stability and reliability of wireless network, has been extensively studied in hybrid RF-FSO communication systems [7]–[10]. The authors in [7] investigated the OP, BER, and EC for a multi-relaying RF-FSO system by taking co-channel interference into account. The effects of outdated CSI on the OP and BER performance for RF-FSO systems with a partial relay selection (PRS) scheme were analyzed in [8]. In [9], the authors considered an asymmetric cognitive RF-FSO network with an additional RF link between a source and a destination, and studied the outage performance under both cognitive and non-cognitive radio scenarios with a PRS strategy. Considering the features of high rate for FSO systems, the authors in [10] considered both ideal and non-ideal hardware cases with a PRS scheme in hybrid RF-FSO systems.

Multi-aperture scheme is usually recognized as a viable technique to migrate the effect of atmospheric turbulence in FSO systems [11]–[14]. In [11], the average capacity for a multiple-input multiple-output (MIMO) FSO system over Gamma-Gamma ($\Gamma\Gamma$) channel was studied, in which the sum of several independent and identical distributed (i.i.d.) $\Gamma\Gamma$ random variables (RVs) was approximated by another $\Gamma\Gamma$ RV. Milosevic *et al* in [12] studied the average BER for a FSO system with a multi-aperture receiver over Málaga ($\mathcal{M}$)-distributed fading channel with pointing errors. The transmission laser selection and repetition coding schemes for a MIMO FSO system were evaluated in [13]. To reduce the impacts of turbulence-induced correlated channel, a polar-coded scheme with and without spatially correlated fading was proposed in [14].

In order to enhance the wireless security, the issue of physical-layer security, which is to utilize the inherent randomness of wireless channel to guarantee the security in physical layer, has attracted increasingly attention from both academia and industry [15], [16], and several works in literature introduced this issue into hybrid RF-FSO systems [17]–[22]. Under Nakagami-m - $\Gamma\Gamma$ fading channels, the secrecy performance in terms of secrecy outage probability (SOP) and average secrecy capacity (ASC) were analyzed in [17]. In [18], the intercept probability for a multiuser SIMO mixed RF-FSO system with multi-antenna relaying and multi-eavesdropping was studied. Adopting a best relay selection scheme and considering the underlay cognitive radio scenario, secrecy performance for a RF-FSO system was investigated in [19]. However, all of aforementioned works, i.e., [17]–[19], just consider the scenario that the RF link is wiretapped because of the high-security of FSO link. Due to the inherent impairments of FSO systems, i.e., the random optical irradiance fluctuations and laser-beam divergence, the FSO link may be also wiretapped and only a few works considered this issue [20]–[22]. The authors in [20] studied the probability of strictly positive secrecy capacity (SPSC) for a FSO system under two intercept scenarios, i.e., the eavesdropper near the transmitter and near the receiver. The closed-form expressions for the ASC, SOP, and the probability of SPSC for a FSO system were derived over $\mathcal{M}$ turbulence fading channel in [21]. Assuming the FSO link was wiretapped, the secrecy performance for a dual hop hybrid RF-FSO system was studied in [22].

Observed from above literature, adopting the multi-relaying and multi-aperture schemes can effectively reduce the turbulence-induced fading and improve the system performance, and these advantages can be integrated by a multi-relaying RF-FSO system with a multi-aperture receiver. Moreover, it is also interesting and promising to take account the physical-layer security issue into this system to enhance the secrecy performance. To the author's best knowledge, such issue has not been investigated in the existing literature.

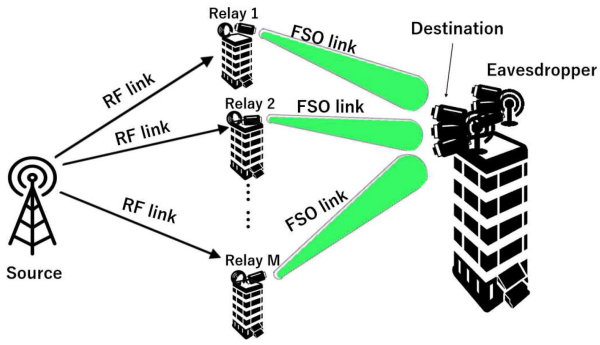

Fig. 1. System model.

Motivated by the aforementioned observations, in this paper, we evaluate the secrecy performance of a multi-relaying mixed RF-FSO system with a multi-aperture receiver in the presence of an eavesdropper. In particular, the physical-layer security of the considered system is studied in terms of SOP and probability of SPSC, while considering the PRS scheme at the relays and the equal gain combining (EGC) scheme at the receiver. Note that EGC is used to process multiple copies of received signal, as it has a good trade-off between performance gain and implementation complexity [23]. The main contributions of this paper are described as follows:

1) We have investigated the physical-layer security performance of a multi-relaying mixed RF-FSO system with a multi-aperture receiver over Nakagami-m - $\Gamma\Gamma$ fading channels, where the FSO link is eavesdropped, as the eavesdropper may be located in the region of laser-beam divergences of the legitimate node.

2) The probability density functions (PDFs) and cumulative distribution functions (CDFs) of the instantaneous SNRs with PRS at the relays and EGC at the receiver have been derived. Utilizing those statistic distributions, we have derived the closed-form expressions for the lower bound of SOP and the probability of SPSC.

3) The accuracy of the analytical results have been verified by Monte-Carlo simulations, and the effects of the number of the relays and apertures as well as atmospheric turbulence on the system performance have been also analyzed.

2. System and Channel Model

2.1 System Model

Fig. 1 shows an asymmetric multi-relaying RF-FSO system, which consists a single-antenna source (S), M parallel single-antenna and single-aperture relays R_m, ($m \in \{1, 2, ..., M\}$), a N-aperture destination (D) and a N-aperture eavesdropper (E). The whole communication process can be separated into two equal time slots. In the first time slot, S broadcasts the confidential information to all the M relays though RF links, and a best relay, selected by the PRS strategy in terms of the maximum instantaneous channel gain for the RF link, is used to assist the transmission from S to D base on a decode-and-forward (DF) protocol. In the second time slot, the selected relay converts the decoded signal to an optical signal, and forwards it to D over FSO channel by using On-Off keying modulation scheme. We assume that all the RF channels are experience i.i.d. Nakagami-m fading and all the FSO channels are subject to i.i.d. $\Gamma\Gamma$ process. It is also assumed that there is no misalignment between the relays and D for the FSO links, meaning the effect of pointing errors is not taking into account. Moreover, the EGC scheme is used to process the multiple copies of the received signals at D and E. It is also assumed that the FSO link is wiretapped by E, as it is located in the region of laser beam divergences of D [20], [22]. We further assume that the received irradiance among all the receiving apertures are uncorrelated as the spatial separation of the photodetectors are greater than the spatial coherence distance of irradiance [12].

In the first time slot, the received signal at m-th relay, R_m, can be written as

$$y_m = \sqrt{P_s} h_{SR_m} x + n_m, \tag{1}$$

where P_s is the transmission power at S, h_{SR_m} is the channel coefficient between S and R_m, x is the transmitted confidential information, and n_m is the additive white Gaussian noise (AWGN) with zero mean and a variance of N_0. The instantaneous SNR at R_m can be expressed as

$$\gamma_{R_m} = P_s |h_{SR_m}|^2 / N_0 = \mu_\gamma |h_{SR_m}|^2, \tag{2}$$

where $\mu_\gamma = P_s/N_0$ is the average SNR. Due to the PRS strategy, the relay with a best instantaneous channel gain of RF link is selected

$$R_m^* = \arg \max_{m \in \{1,\ldots,M\}} |h_{SR_m}|^2. \tag{3}$$

Therefore, the instantaneous SNR at the best relay, R_m^*, is

$$\gamma_{R_m^*} = \mu_\gamma \max_{m \in \{1,\ldots,M\}} |h_{SR_m}|^2. \tag{4}$$

Since all of the RF links are assumed to be i.i.d., the CDF and PDF of $\gamma_{R_m^*}$ can be given by

$$F_{\gamma_{R_m^*}}(x) = [F_{\gamma_{R_m}}(x)]^M, \tag{5}$$

and

$$f_{\gamma_{R_m^*}}(x) = M[F_{\gamma_{R_m}}(x)]^{M-1} f_{\gamma_{R_m}}(x), \tag{6}$$

where $F_\gamma(\cdot)$ and $f_\gamma(\cdot)$ denote the CDF and PDF of γ, respectively.

In the second time slot, D converts the received optical signal to the electrical one, and the received electrical signal at the output of the n-th photodetector is given by

$$r_{nk} = \frac{x_{R_m^*} \zeta I_{nk}}{N} + z_{nk}, \tag{7}$$

where $x_{R_m^*} \in \{0, 1\}$ represents the information forwarded by R_m^*, ζ is the optical-to-electrical conversion coefficient, I_{nk} denotes the normalized received irradiance between R_m^* and n-th aperture of link k, $k \in \{D, E\}$, z_{nk} is the AWGN with zero mean and a variance of N_0. For a fair comparison, the factor N is used to ensure the receiver aperture areas is same between single-input single-output and SIMO scenarios [11]. The instantaneous electrical SNR at the n-th aperture can be written as

$$\gamma_{nk} = \zeta^2 I_{nk}^2 / N_0 = \bar{\gamma}_{nk} I_{nk}^2, \tag{8}$$

where $\bar{\gamma}_{nk}$ is the average SNR. The output signal at the EGC receiver is

$$r_k = \frac{x_{R_m^*} \zeta}{N} \sum_{n=1}^{N} I_{nk} + \xi_k, \tag{9}$$

where ξ_k is the total receiving noise at k. We have the instantaneous electrical SNR at k as

$$\gamma_k = \frac{\zeta^2 I_k^2}{N^2 N_0} = \bar{\gamma}_k {I_k}^2, \tag{10}$$

where $I_k = \sum_{n=1}^{N} I_{nk}$ denotes the combined irradiance of the receiver, and $\bar{\gamma}_k = \frac{\zeta^2}{N N_0}$ denotes the average SNR.

2.2 Fading Channel Model

In this paper, all the RF channels are assumed to experience i.i.d. quasi-static Nakagami-m fading with fading parameter m. Thus, the channel power gain, $|h_{SR_m}|^2$, follows the i.i.d. gamma distributed

with parameter m. Hence, the PDF and CDF of $|h_{SR_m}|^2$ can be expressed as

$$f_{|h_{SR_m}|^2}(x) = \frac{x^{m-1}}{\Gamma(m)}\left(\frac{m}{\Omega}\right)^m e^{-(\frac{m}{\Omega})x}, \tag{11}$$

and

$$F_{|h_{SR_m}|^2}(x) = 1 - \frac{\Gamma(m, \frac{m}{\Omega}x)}{\Gamma(m)} = 1 - e^{-\frac{m}{\Omega}x}\sum_{n=0}^{m-1}\frac{(\frac{m}{\Omega})^n}{n!}x^n, \tag{12}$$

respectively, where Ω is normalized average power, $\Gamma(\cdot)$ is the Gamma function defined by (8.310.1) in [24], and $\Gamma(a, x) = \int_x^\infty e^{-t}t^{a-1}dt$ is the upper incomplete Gamma function defined by (8.350.2) in [24].

From (2), (11) and (12), we can re-express (5) and (6) as [25]

$$F_{\gamma_{R_m^*}}(\gamma) = \sum_{p=o}^{M}\sum_{q=0}^{(m-1)p}\binom{M}{p}(-1)^p a_q^{p,m}(\gamma\frac{m}{\mu_\gamma})^q e^{-p\gamma\frac{m}{\mu_\gamma}}, \tag{13}$$

and

$$f_{\gamma_{R_m^*}}(\gamma) = M\sum_{p=o}^{M-1}\sum_{q=0}^{(m-1)p}\binom{M-1}{p}(-1)^p a_q^{p,m}\left(\frac{m}{\mu_\gamma}\right)^{q+m}\frac{\gamma^{q+m-1}}{\Gamma(m)}e^{-(p+1)\gamma\frac{m}{\mu_\gamma}}, \tag{14}$$

respectively.

Due to the FSO link is modeled by a $\Gamma\Gamma$ fading, the PDF of the irradiance, I_{nk}, is given by

$$f_{I_n}(x) = \frac{2(\alpha\beta)^{(\alpha+\beta)/2}}{\Gamma(\alpha)\Gamma(\beta)}I_n^{(\alpha+\beta)/2-1}K_{\alpha-\beta}(2\sqrt{\alpha\beta I_n}), \tag{15}$$

where $K_v(\cdot)$ is the modified Bessel function of the second kind of order $\alpha - \beta$, and α and β are the PDF parameters that describes the turbulence induced by waves, and in the case of zero-inner scale [26], they are given by

$$\alpha = \left\{\exp\left[\frac{0.49\sigma^2}{(1+0.18\chi^2+0.56\sigma^{12/5})^{7/6}}\right]-1\right\}^{-1}, \beta = \left\{\exp\left[\frac{0.51\sigma^2}{(1+0.9\chi^2+0.62\sigma^{12/5})^{5/6}}\right]-1\right\}^{-1}, \tag{16}$$

where $\sigma^2 = 1.23C_n^2k^{7/6}L^{11/6}$ is the Rytov variance, L is link distance, $k = 2\pi/\lambda$ is the optical wave number with $\chi = (\sigma\varrho^2/4L)^{1/2}$, ϱ is the diameter of receiver aperture, and C_n^2 is the turbulence strength factor [27].

Next, we re-write $K_v(\cdot)$ into the form of Meijers G-function, which is defined by (9.34.3) in [24], as

$$f_{I_n}(x) = \frac{\alpha\beta}{\Gamma(\alpha)\Gamma(\beta)}G_{0,2}^{2,0}\left[\alpha\beta x\middle|\begin{matrix}\\ \alpha-1, \beta-1\end{matrix}\right]. \tag{17}$$

Therefore, the corresponding CDF can be expressed as

$$F_{I_n}(x) = \frac{1}{\Gamma(\alpha)\Gamma(\beta)}G_{1,3}^{2,1}\left[\alpha\beta\sqrt{x}\middle|\begin{matrix}1\\ \alpha, \beta, 0\end{matrix}\right]. \tag{18}$$

Since all the FSO channels are modeled as i.i.d. $\Gamma\Gamma$ fading, the sum of received irradiance, I_k, can be approximated by another $\Gamma\Gamma$ RV, I_s, as

$$I_k \approx I_s \sim \Gamma\Gamma(\alpha_s, \beta_s, \Omega_s) \tag{19}$$

where α_s and β_s are given as

$$\alpha_s = N\alpha + \varepsilon \tag{20}$$

and

$$\beta_s = N\beta, \tag{21}$$

in which ε is an adjustment parameter, which is used to improve the accuracy of the proposed approximation [28], and it can be given as

$$\varepsilon = (N-1)\frac{-0.127 - 0.95\alpha - 0.0058\beta}{1 + 0.00124\alpha + 0.98\beta}. \tag{22}$$

Using (10), (17), (18), and (19), the PDF and CDF of γ_k can be derived as

$$f_{\gamma_k}(\gamma_k) = \frac{(\frac{\alpha_s\beta_s}{N})^2}{2\Gamma(\alpha_s)\Gamma(\beta_s)\bar{\gamma}_k} G_{0,2}^{2,0}\left[\frac{\alpha_s\beta_s}{N}\sqrt{\frac{\gamma_k}{\bar{\gamma}_k}}\middle|\alpha_s - 2, \beta_s - 2\right] \tag{23}$$

and

$$F_{\gamma_k}(\gamma_k) = \frac{1}{\Gamma(\alpha_s)\Gamma(\beta_s)} G_{1,3}^{2,1}\left[\frac{\alpha_s\beta_s}{N}\sqrt{\frac{\gamma_k}{\bar{\gamma}_k}}\middle|\begin{matrix}1\\ \alpha_s, \beta_s, 0\end{matrix}\right], \tag{24}$$

respectively.

3. Secrecy Performance Analysis

In the content of physical-layer security, ASC, SOP, and the probability of SPSC are commonly used performance metrics to study the secrecy in fading channels. Due to fact that the closed-form expression of ASC is mathematically intractable for our considered system, therefore, we only focus on SOP and the probability of SPSC in this section.

3.1 SOP

As defined in [29], the instantaneous secrecy capacity (SC) of the system using DF relaying scheme is

$$C_s = \min(C_{SR_m^*}, C_{R_m^*D}), \tag{25}$$

where $C_{SR_m^*}$ and $C_{R_m^*D}$ are the SC of S-R_m^* and R_m^*-D links, respectively, which can be expressed as

$$C_{SR_m^*} = \frac{1}{2}\log_2(1 + \gamma_{R_m^*}), \tag{26}$$

and

$$C_{R_m^*D} = \left\{\frac{1}{2}(\log_2(1 + \gamma_D) - \log_2(1 + \gamma_E))\right\}^+, \tag{27}$$

where $\{x\}^+$=max$\{x, 0\}$. Secrecy outage occurs when the instantaneous SC falls below a target SC, C_{th} ($C_{th} \geq 0$). Thus, SOP is defined as a probability that the instantaneous SC is smaller than C_{th} [30]. Therefore, we have

$$P_{SOP} = Pr\{C_s < C_{th}\} = 1 - Pr\{C_{SR_m^*} \geq C_{th}\}Pr\{C_{R_m^*D} \geq C_{th}\}. \tag{28}$$

Substituting (13), (23) and (24) into (28), SOP can be re-expressed as

$$P_{SOP} = 1 - \left[1 - F_{\gamma_{R_m^*}}(\Theta - 1)\right]\left[1 - \int_0^\infty F_{\gamma_D}(\Theta\gamma_E + \Theta - 1)f_{\gamma_E}(\gamma_E)d\gamma_E\right], \tag{29}$$

where $\Theta = 2^{2C_{th}}$. Note that the exact closed-form expression for SOP as show in (29) is mathematically difficult to be obtained. Alternatively, we evaluate the lower bound of SOP. For the case when $\gamma_E \to \infty$, the lower bound of SOP can be given by

$$P_{SOP} \geq P_{SOP_L} \triangleq 1 - \left[1 - F_{\gamma_{R_m^*}}(\Theta - 1)\right]\left[1 - \int_0^\infty F_{\gamma_D}(\Theta\gamma_E)f_{\gamma_E}(\gamma_E)d\gamma_E\right]. \tag{30}$$

Making use of (07.34.21.0011.01) in [31], we have

$$PSOP_L = \sum_{p=o}^{M}\sum_{q=0}^{(m-1)p}\binom{M}{p}(-1)^p a_q^{p,m}\left(\frac{(\Theta-1)m}{\mu_\gamma}\right)^q e^{-p(\Theta-1)\frac{m}{\mu_\gamma}} + \left(1-\sum_{p=o}^{M}\sum_{q=0}^{(m-1)p}\binom{M}{p}(-1)^p \times a_q^{p,m}\left(\frac{(\Theta-1)m}{\mu_\gamma}\right)^q e^{-p(\Theta-1)\frac{m}{\mu_\gamma}}\right)\frac{1}{\Gamma^2(\alpha_s)\Gamma^2(\beta_s)}\frac{\bar{\gamma}_D}{\Theta\bar{\gamma}_E}G_{3,3}^{3,2}\left[\sqrt{\frac{\bar{\gamma}_D}{\Theta\bar{\gamma}_E}}\middle|\begin{matrix}-1-\alpha_s,-1-\beta_s,-1\\ \alpha_s-2,\beta_s-2,-2\end{matrix}\right]. \quad (31)$$

3.2 Probability of SPSC

Furthermore, the SPSC is another essential criterion for physical-layer security, which is used to emphasize the existence of SC, and the probability of SPSC is defined as a probability that SC is greater than zero. Therefore, we have

$$\begin{aligned} P_{SPSC} &= Pr\{C_s > 0\} \\ &= Pr\{\min(C_{SR_m^*}, C_{R_m^*D}) > 0\} \\ &= Pr\{C_{SR_m^*} > 0\}Pr\{C_{R_m^*D} > 0\} \end{aligned} \quad (32)$$

where

$$\begin{aligned} Pr\{C_{SR_m^*} > 0\} &= Pr\left\{\frac{1}{2}\log_2(1+\gamma_{R_m^*}) > 0\right\} \\ &= Pr\{\gamma_{R_m^*} > 0\} \\ &= \int_0^\infty f_{\gamma_{R_m^*}}(\gamma)d\gamma \\ &= 1, \end{aligned} \quad (33)$$

and

$$\begin{aligned} Pr\{C_{R_m^*D} > 0\} &= Pr\left\{\frac{1}{2}(\log_2(1+\gamma_D) - \log_2(1+\gamma_E)) > 0\right\} \\ &= Pr\{\gamma_D > \gamma_E\} \\ &= 1 - \int_0^\infty F_{\gamma_D}(\gamma_E) f_{\gamma_E}(\gamma_E)d\gamma_E \\ &= 1 - \int_0^\infty \frac{1}{\Gamma(\alpha_s)\Gamma(\beta_s)}G_{1,3}^{2,1}\left[\frac{\alpha_s\beta_s}{N}\sqrt{\frac{\gamma_E}{\bar{\gamma}_D}}\middle|\begin{matrix}1\\ \alpha_s,\beta_s,0\end{matrix}\right] \\ &\quad \times \frac{(\frac{\alpha_s\beta_s}{N})^2}{2\Gamma(\alpha_s)\Gamma(\beta_s)\bar{\gamma}_E}G_{0,2}^{2,0}\left[\frac{\alpha_s\beta_s}{N}\sqrt{\frac{\gamma_E}{\bar{\gamma}_E}}\middle|\alpha_s-2,\beta_s-2\right]d\gamma_E. \end{aligned} \quad (34)$$

Making use of (07.34.21.0011.01) in [31] and after some manipulations, it has

$$P_{SPSC} = 1 - \frac{\bar{\gamma}_D}{\Gamma^2(\alpha_s)\Gamma^2(\beta_s)\bar{\gamma}_E}G_{3,3}^{3,2}\left[\sqrt{\frac{\bar{\gamma}_D}{\bar{\gamma}_E}}\middle|\begin{matrix}-1-\alpha_s,-1-\beta_s,-1\\ \alpha_s-2,\beta_s-2,-2\end{matrix}\right]. \quad (35)$$

4. Numerical Results and Discussions

In this section, numerical and Monte-Carlo simulations results are presented. Similar to [17] and [22], following combinations are used to represent three typical turbulence conditions: $\alpha_D = \alpha_E = 2.902$, $\beta_D = \beta_E = 2.510$ (weak turbulence), $\alpha_D = \alpha_E = 2.296$, $\beta_D = \beta_E = 1.822$ (moderate turbulence), and $\alpha_D = \alpha_E = 2.064$, $\beta_D = \beta_E = 1.342$ (strong turbulence). Without loss of generality, we also set $m = 3$ and $\zeta = 1$ in those results.

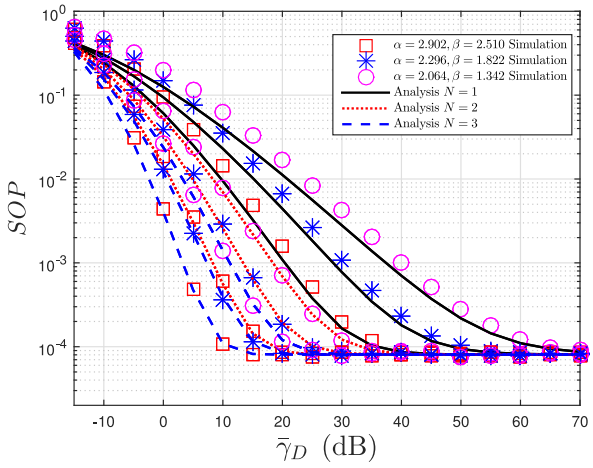

Fig. 2. SOP versus $\bar{\gamma}_D$ with $M = 2$, $\mu_\gamma = -10$ dB, $\bar{\gamma}_E = -18$ dB, and C_{th}=0.01 bits/s/Hz.

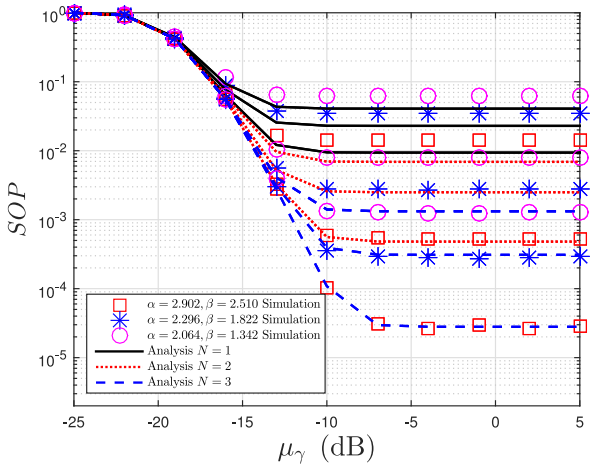

Fig. 3. SOP versus μ_γ with $M = 2$, $\bar{\gamma}_D = 10$ dB, $\bar{\gamma}_E = -18$ dB, and C_{th}=0.01 bits/s/Hz.

Fig. 2 shows the SOP versus $\bar{\gamma}_D$ under different number of apertures and atmospheric turbulence conditions. It is observed that the secrecy performance improves as $\bar{\gamma}_D$ increases, as the channel condition of R_m^*-D link is superior to that of R_m^*-E link. However, there is a flat area for the curve in this figure, and the values of SOP remain unchanged when $\bar{\gamma}_D$ is beyond a certain value, i.e., $\bar{\gamma}_D > 30$ dB when $N = 3$. This is because in the dual-hop DF-based relaying network, the system performance is dominated by the worse hop, and when $\bar{\gamma}_D$ is high, the system capacity is limited by the first hop, which is not improved. In addition, we observe that the secrecy performance with a higher N outperforms that with a lower one when $\bar{\gamma}_D$ is in the low-to-medium range, due to the advantage of employing multi-aperture scheme. However, when $\bar{\gamma}_D$ is in the high range (i.e., $\bar{\gamma}_D >$ 70 dB), all curves converge into one, as the system performance is dominated by the first hop and the improvement of the channel condition in the second hop is insignificant. Moreover, the results also shows that the system performance decreases as the turbulence gets severe.

In Fig. 3, the influence of μ_γ on the SOP performance with various number of apertures is illustrated. It can be noticed that there is also a floor in this figure due to the fact that the second hop is dominated when μ_γ is high.

Fig. 4 depicts the effect of the number of the relays on SOP performance. We can observe that under the same turbulence condition, employing more relays leads to better SOP performance when the channel of the first hop is comparably weak (i.e., $\mu_\gamma < -5$ dB). However, when it gets

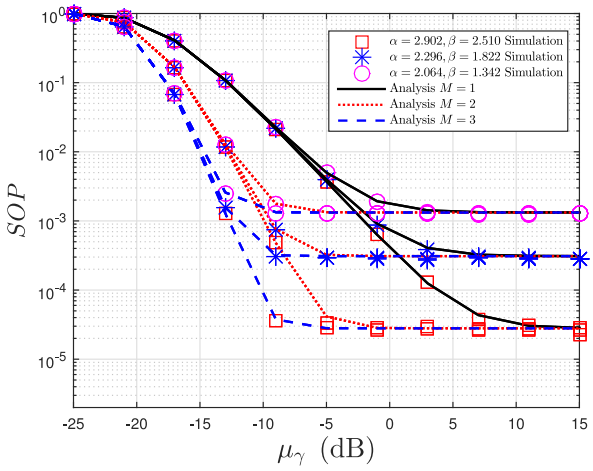

Fig. 4. SOP versus μ_γ with $N = 3$, $\bar{\gamma}_D = 10$ dB, $\bar{\gamma}_E = -18$ dB, and C_{th}=0.01 bits/s/Hz.

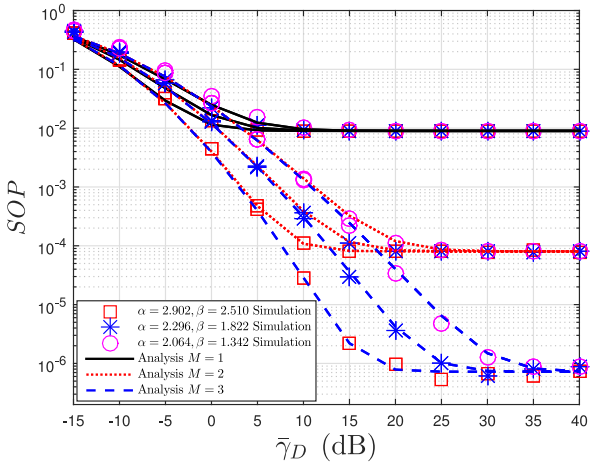

Fig. 5. SOP versus $\bar{\gamma}_D$ with $N = 3$, $\mu_\gamma = -10$ dB, $\bar{\gamma}_E = -18$ dB, and C_{th}=0.01 bits/s/Hz.

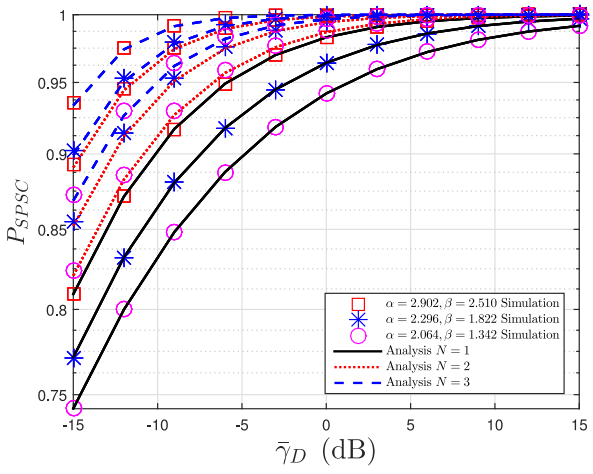

Fig. 6. Probability of SPSC versus $\bar{\gamma}_D$ with $N = 1,2,3$, $\bar{\gamma}_E = -25$ dB.

better (i.e., $\mu_\gamma > 10$ dB), employing different numbers of the relays results in the same SOP performance. This is because the system performance is dominated by the second hop, and the advantage of multi-relaying technique is insignificant when μ_γ is large.

As depicted in Fig. 5, the SOP versus $\bar{\gamma}_D$ is presented. From this figure, the advantage of using multi-relaying scheme is very obvious when $\bar{\gamma}_D$ is large due to the first hop dominates the performance.

Fig. 6 illustrates the effects of various apertures and turbulence conditions on the probability of SPSC. We can observe that the system performance improves when $\bar{\gamma}_D$ increases, as R_m^*-D link gets better than R_m^*-E link. Moreover, the probability of SPSC increases as more apertures are used under the same turbulence condition, which further demonstrates that multi-aperture receiving strategy can enhance the secrecy performance.

Finally, we can observe that simulation results match well with the analytical ones in all considered cases, which validates our analytical expressions derived.

5. Conclusion

In this paper, we have studied the secrecy performance for an asymmetric RF-FSO communication system, in which the FSO link is wiretapped. Moreover, the multi-relaying and multi-aperture receiving schemes are also considered to enhance the system performance. Assuming all the RF and FSO links experience i.i.d. fading, the exact expressions of the PDF and CDF for SNR have been derived. Utilizing those statistic distributions, we have derived the expressions for the lower bound of SOP and the probability of SPSC. Furthermore, the effects of atmospheric turbulence, the number of the relays and apertures on the secrecy performance have been also studied. The accuracy of our derivations are verified by Monte Carlo simulation, and the results shows that employing more relays and apertures can greatly improve the secrecy performance when the first and second hop dominates the system performance, respectively.

References

[1] H. Kaushal and G. Kaddoum, "Optical communication in space: Challenges and mitigation techniques," *IEEE Commun. Surv. Tut.*, vol. 19, no. 1, pp. 57–96, Feb. 2017.
[2] M. A. Khalighi and M. Uysal, "Survey on free space optical communication: A communication theory perspective," *IEEE Commun. Surv. Tut.*, vol. 16, no. 4, pp. 2231–2258, Jun. 2014.
[3] W. M. R. Shakir, "On performance analysis of hybrid FSO/RF systems," *IET Commun.*, vol. 13, no. 11, pp. 1677–1684, Jul. 2019.
[4] E. Zedini, I. S. Ansari, and M.-S. Alouini, "Performance analysis of mixed Nakagami-*m* and Gamma-Gamma dual-hop FSO transmission systems," *IEEE Photon. J.*, vol. 7, no. 1, Dec. 2014, Art. no. 7900120.
[5] E. S. Altubaishi and K. Alhamawi, "Capacity analysis of hybrid AF multi-hop FSO/RF system under pointing errors and weather effects," *IEEE Photon. Technol. Lett.*, vol. 31, no. 15, pp. 1304–1307, Aug. 2019.
[6] B. Bag, A. Das, I. S. Ansari, A. Prokeš, C. Bose, and A. Chandra, "Performance analysis of hybrid FSO systems using FSO/RF-FSO link adaptation," *IEEE Photon. J.*, vol. 10, no. 3, Jun. 2018, Art. no. 7904417.
[7] E. Balti and M. Guizani, "Mixed RF/FSO cooperative relaying systems with co-channel interference," *IEEE Trans. Commun.*, vol. 66, no. 9, pp. 4014–4027, Sep. 2018.
[8] M. I. Petkovic, A. M. Cvetkovic, G. T. Djordjevic, and G. K. Karagiannidis, "Partial relay selection with outdated channel state estimation in mixed RF/FSO systems," *J. Lightw. Technol.*, vol. 33, no. 13, pp. 2860–2867, Jul. 2015.
[9] H. Arezumand, H. Zamiri-Jafarian, and E. Soleimani-Nasab, "Exact and asymptotic analysis of partial relay selection for cognitive RF-FSO systems with non-zero boresight pointing errors," *IEEE Access*, vol. 7, pp. 58611–58625, May 2019.
[10] E. Balti, M. Guizani, B. Hamdaoui, and Y. Maalej, "Partial relay selection for hybrid RF/FSO systems with hardware impairments," in *Proc. IEEE GLOBECOM*, Dec. 2016, pp. 1–6.
[11] D. A. Luong and A. T. Pham, "Average capacity of MIMO free-space optical Gamma-Gamma fading channel," in *Proc. IEEE Int. Conf. Commun.*, Jun. 2014, pp. 3354–3358.
[12] N. D. Milosevic, M. I. Petkovic, and G. T. Djordjevic, "Average BER of SIM-DPSK FSO system with multiple receivers over $\mathcal{M}$-distributed atmospheric channel with pointing errors," *IEEE Photon. J.*, vol. 9, no. 4, Aug. 2017, Art. no. 6601210.
[13] C. Abou-Rjeily *et al.*, "Performance analysis of FSO communications with diversity methods: Add more relays or more apertures?" *IEEE J. Sel. Areas Commun.*, vol. 33, no. 9, pp. 1890–1902, Sep. 2015.
[14] J. Fang *et al.*, "Polar-coded MIMO FSO communication system over Gamma-Gamma turbulence channel with spatially correlated fading," *IEEE/OSA J. Opt. Commun. Netw.*, vol. 10, no. 11, pp. 915–923, Nov. 2018.

[15] J. Zhang and G. Pan, "Secrecy outage analysis with *k*th best relay selection in dual-hop inter-vehicle communication systems," *AEU-Int. J. Electron. Commun.*, vol. 71, pp. 139–144, Jan. 2017.
[16] G. Pan, J. Ye, and Z. Ding, "Secure hybrid VLC-RF systems with light energy harvesting," *IEEE Trans. Commun.*, vol. 65, no. 10, pp. 4348–4359, Oct. 2017.
[17] H. Lei, Z. Dai, I. S. Ansari, K.-H. Park, G. Pan, and M.-S. Alouini, "On secrecy performance of mixed RF-FSO systems," *IEEE Photon. J.*, vol. 9, no. 4, Aug. 2017, Art. no. 7904814.
[18] A. H. A. El-Malek, A. M. Salhab, S. A. Zummo, and M.-S. Alouini, "Enhancing physical layer security of multiuser SIMO mixed RF/FSO relay networks with multi-eavesdroppers," in *Proc. IEEE Globecom Workshops*, Feb. 2017, pp. 1–7.
[19] M. Torabi and A. B. Pouri, "Physical layer security of a two-hop mixed RF-FSO system in a cognitive radio network," in *Proc. 2nd West Asian Colloq. Opt. Wireless Commun.*, Tehran, Iran, Jul. 2019, pp. 167–170.
[20] F. J. Lopez-Martinez, G. Gomez, and J. M. Garrido-Balsells, "Physical-Layer security in free-space optical communications," *IEEE Photon. J.*, vol. 7, no. 2, Apr. 2015, Art. no. 7901014.
[21] M. J. Saber and S. M. S. Sadough, "On secure free-space optical communications over Málaga turbulence channels," *IEEE Wireless Commun. Lett.*, vol. 6, no. 2, pp. 274–277, Apr. 2017.
[22] X. Pan, H. Ran, G. Pan, Y. Xie, and J. Zhang, "On secrecy analysis of DF based dual hop mixed RF-FSO systems," *IEEE Access*, vol. 7, pp. 66725–66730, May 2019.
[23] H. Samimi, "Equal-gain combining reception over Gamma-Gamma turbulence channels with pointing errors," *IET Optoelectronics*, vol. 8, no. 5, pp. 191–195, Oct. 2014.
[24] I. Gradshteyn and I. Ryzhik, *Table of Integrals, Series and Products*, 7th ed. San Diego, CA, USA: Academic, 2007.
[25] R. Zhao, Y. Yuan, L. Fan, and Y. He, "Secrecy performance analysis of cognitive decode-and-forward relay networks in Nakagami-*m* fading channels," *IEEE Trans. Commun.*, vol. 65, no. 2, pp. 549–563, Feb. 2017.
[26] H. Khanna, M. Aggarwal, and S. Ahuja, "Statistical characteristics and performance evaluation of FSO links with misalignment fading influenced by correlated sways," *AEU-Int. J. Electron. Commun.*, vol. 85, pp. 118–125, Feb. 2018.
[27] J. Vellakudiyan, P. Muthuchidambaranathan, F. M. Bui, and V. Palliyembil, "Performance of a subcarrier intensity modulated differential phase-shift keying over generalized turbulence channel," *AEU-Int. J. Electron. Commun.*, vol. 69, no. 11, pp. 1569–1573, Nov. 2015.
[28] N. D. Chatzidiamantis and G. K. Karagiannidis, "On the distribution of the sum of Gamma-Gamma variates and applications in RF and optical wireless communications," *IEEE Trans. Commun.*, vol. 59, no. 5, pp. 1298–1308, May 2011.
[29] M. Bloch, J. Barros, M. R. Rodrigues, and S. W. McLaughlin, "Wireless information-theoretic security," *IEEE Trans. Inf. Theory*, vol. 54, no. 6, pp. 2515–2534, Jun. 2008.
[30] G. Pan, J. Ye, and Z. Ding, "On secure VLC systems with spatially random terminals," *IEEE Commun. Lett.*, vol. 21, no. 3, pp. 492–495, Mar. 2017.
[31] Wolfram, The wolfram functions site, 2001. [Online]. Available: http://functions.wolfram.com